

Effects of modal coupling on the nonlinear dynamics of hyperelastic circular cylindrical shells

Daniella M. O. Aguiar¹, Renata M. Soares¹, Frederico M. A. da Silva¹

¹*School of Civil and Environmental Engineering, Federal University of Goiás
Avenida Universitária, 1488, Qd. 86, Setor Leste Universitário, 74605-220, Goiás, Brasil
daniella.aguiar@discente.ufg.br, renatasoares@ufg.br, silvafma@ufg.br*

Abstract. The nonlinear dynamics of a simply supported circular cylindrical shell is analyzed using an analytical model that considers both physical and geometrical nonlinearities. The material that composes the shell is assumed as homogeneous, isotropic, hyperelastic and incompressible, being described by the Mooney-Rivlin hyperelastic constitutive law. The geometric nonlinearity is introduced into the analytical model by applying the Sanders-Koiter's nonlinear shell theory. The Rayleigh-Ritz method and Hamilton's principle are employed to obtain the nonlinear equilibrium equations. For that, the energy density function is expanded in Taylor series up to the fourth order and the transversal displacement field is described in Fourier series that considers both asymmetric and axisymmetric modes. This work focusses on evaluating the influence of the asymmetric, axisymmetric, and companion modes, selected in the modal solution of the displacement fields, on the resonance curve of the shell. It can be observed that when the axisymmetric and companion modes are added, there is a significant change in the nonlinear behavior of the hyperelastic shell - which indicates the importance of these modal coupling in the nonlinear dynamic analysis.

Keywords: Hyperelastic material, Cylindrical shell, Nonlinear dynamic, Asymmetric modes, Axisymmetric modes

1 Introduction

The consideration of linear elastic behavior is applicable only to small deformations. However, many structures show large deformations, depending on the load or even the type of material they are made. In soft materials, such as rubbers and biological tissues, nonlinear elastic behavior is predominant. Hyperelastic models, based on the deformation energy density function, have come about as a result of the need to model this kind of material, which has become more popular with the development of materials science.

Due to their large bearing capacity of load and high stiffness-to-weight ratio, shells are widely used as structural elements in many areas. Hyperelastic shells are currently found in the aerospace industry (solid fuel tank for rockets), mechanics (vibration and shock absorbers), biomechanics (prostheses and implants, biological tissue modelling), medicine (surgical and medical supplies) and robotics (soft and industrial robots).

As a result, many researchers have worked to evaluate the behavior of hyperelastic shells. The recent study by Khaniki and Ghayesh [1] investigates the statics and dynamics of cylindrical, spherical, double-curved and hyperbolic hyperelastic shells. The Mooney-Rivlin hyperelastic constitutive law and Donnell's nonlinear shell theory with application of the Hamilton principle are applied to obtain the equilibrium equations. Some of the presented analyses include the effects of curvature on elastic deformation, natural frequencies and forced vibration.

Arani et al. [2] analyze the effect of geometric and material parameters on the vibration of a thin circular cylindrical shell. The material of the shell is of the Mooney-Rivlin type and, in order to reduce the number of degrees of freedom in the system of equations, the static condensation method is applied. The equations in undamped free vibration are examined using the Lindstedt-Poincaré technique. For the system of equations under radial harmonic excitation and damping, the multiscale method is applied. The natural frequencies, backbones and amplitude response for asymmetric and axisymmetric modes are presented.

Zheng et al. [3] show a qualitative and quantitative analysis of the vibrations in a thin hyperelastic cylindrical shell under radial harmonic excitation using the modified Lindstedt-Poincaré technique. To consider physical and geometric nonlinearities, the Mooney-Rivlin incompressible model and Donnell's nonlinear shell theory are used. Frequency-amplitude curves, number of equilibrium points, bifurcation diagrams are obtained.

This paper analyzes the nonlinear dynamics of a circular cylindrical shell composed of Mooney-Rivlin hy-

perelastic material using the deformation-displacement relationship given by the Sanders-Koiter nonlinear theory. The system of equations is obtained by applying the Rayleigh-Ritz method, using a modal expansion for the displacement fields that satisfies the boundary conditions of the shell, and the Hamilton principle. These displacement fields are described as a Fourier series and contains asymmetric, axisymmetric, and companion modes. This work aims to evaluate the influence of these selected modes (companion and axisymmetric modes) on the resonance curve of the hyperelastic cylindrical shell. From the numerical results, it can be noted that the addition of axisymmetric and companion modes considerably modifies the behavior of the resonance curve, thus indicating the importance of considering these modes in the forced dynamic analysis.

2 Mathematical formulation

A simply supported circular cylindrical shell, composed of an isotropic, homogeneous, incompressible and hyperelastic material of the Mooney-Rivlin type, is analyzed. The geometry of the shell with thickness h , radius R , length L and density ρ , and the displacement field of the middle surface u , v and w as defined in the axial x , circumferential θ and lateral z directions, in that respective order, are illustrated in Fig. 1. The boundary conditions are shown in eq. (1), where u , v and w are the axial, circumferential and transversal displacement fields, respectively, and, M_x and N_x are the internal axial bending moment and axial membrane force, respectively.

$$u_{,x} = v = w = M_x = N_x = 0 \quad \text{at } x = 0, L. \quad (1)$$

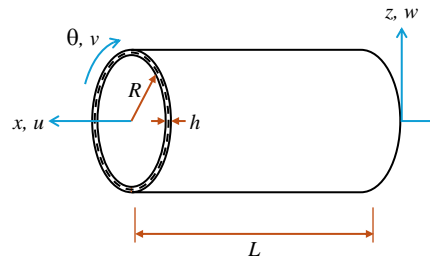


Figure 1. The cylindrical shell geometry, the coordinate system and the displacement fields.

The Lagrange equations, eq. (2), are used to describe the behavior of the shell, where $Lag = T - \Pi$ being T , eq. (3), the kinetic energy, Π , eq. (4), the internal potential deformation energy, and N is the number of generalized coordinates q_k .

$$\frac{d}{dt} \left(\frac{\partial Lag}{\partial \dot{q}_k} \right) - \left(\frac{\partial Lag}{\partial q_k} \right) = Q_k, \quad k = 1 \dots N. \quad (2)$$

$$T = \frac{\rho h}{2} \int_0^L \int_0^{2\pi} (\dot{u}^2 + \dot{v}^2 + \dot{w}^2) R d\theta dx. \quad (3)$$

$$\Pi = \int_0^L \int_0^{2\pi} \int_{-\frac{h}{2}}^{\frac{h}{2}} W R dz d\theta dx. \quad (4)$$

$$Q_k = -\frac{\partial R_e}{\partial \dot{q}_k} + \frac{\partial W_e}{\partial q_k}. \quad (5)$$

The generalized force Q_k in eq. (5) is represented by both the non-conservative damping force, R_e , and the virtual work done by the external forces, W_e . The non-conservative damping force R_e , eq. (6), is viscous damping force where β_1 is its damping coefficient. The virtual work done by the external forces W_e is set in this study by eq. (7) as the same shape of the natural vibration mode, being p the magnitude of the transversal pressure.

$$R_e = \frac{1}{2} \beta_1 R \int_0^L \int_0^{2\pi} \dot{w}^2 d\theta dx, \quad \beta_1 = 2 \eta_1 \rho h \omega_0. \quad (6)$$

$$W_e = \int_0^L \int_0^{2\pi} P w R d\theta dx, \quad P = p \cos(n\theta) \sin\left(\frac{m\pi x}{L}\right) \cos(\Omega t). \quad (7)$$

It is useful to present the modal solutions used to describe the displacement fields, eq. (8), where $w(x, \theta, t)$, $u(x, \theta, t)$, $v(x, \theta, t)$ are the modal solutions that satisfy the boundary conditions of eq. (1) being described by the following Fourier series:

$$w(x, \theta, t) = \sum_{j=1}^J \sum_{i=1}^I w_{ji}(t) \cos(in\theta) \sin\left(\frac{jm\pi x}{L}\right) + \sum_{j=1}^J \sum_{s=1}^S w_{js}(t) \sin(sn\theta) \cos\left(\frac{jm\pi x}{L}\right) + \sum_{j=1}^J w_{j0}(t) \sin\left(\frac{jm\pi x}{L}\right)$$

$$u(x, \theta, t) = \sum_{j=1}^J \sum_{i=1}^I u_{ji}(t) \cos(in\theta) \cos\left(\frac{jm\pi x}{L}\right) + \sum_{j=1}^J \sum_{s=1}^S u_{js}(t) \sin(sn\theta) \sin\left(\frac{jm\pi x}{L}\right) + \sum_{j=1}^J u_{j0}(t) \cos\left(\frac{jm\pi x}{L}\right) \quad (8)$$

$$v(x, \theta, t) = \sum_{j=1}^J \sum_{i=1}^I v_{ji}(t) \sin(in\theta) \sin\left(\frac{jm\pi x}{L}\right) + \sum_{j=1}^J \sum_{s=1}^S v_{js}(t) \cos(sn\theta) \cos\left(\frac{jm\pi x}{L}\right),$$

where m and n are, respectively, the axial half-wave number and the circumferential wave number of the natural vibration mode; $w_{ji}(t)$, $u_{ji}(t)$, and $v_{ji}(t)$, are the asymmetric modal amplitudes, named as driven modes due to the traversal pressure excites directly these modal amplitudes; $w_{js}(t)$, $u_{js}(t)$, and $v_{js}(t)$ are the companion modal amplitudes that they are indirectly excited by the transversal pressure and they are circumferentially out of phase [4]; and, $w_{j0}(t)$ and $u_{j0}(t)$ are the axisymmetric modal amplitudes. The vector of generalized coordinates is expressed in terms of these modal amplitudes as $q_k = [w_{ij}(t), w_{js}(t), w_{j0}(t), u_{ij}(t), u_{js}(t), u_{j0}(t), v_{ij}(t), v_{js}(t)]$.

Returning to eq. (4), the energy density function, W , incorporates the nonlinear stress-strain relationship into the system and, in this work, is defined by the Mooney-Rivlin hyperelastic constitutive model, as follows:

$$W = \mu_1 (I_1 - 3) + \mu_2 (I_2 - 3), \quad (9)$$

where μ_1 and μ_2 are material parameters; and I_1 and I_2 are the first and second deformation invariants, respectively.

To describe these deformation invariants, the right Cauchy-Green deformation tensor \mathbf{C} is used, and it can be obtained from the Green-Lagrange deformation tensor \mathbf{E} and the identity matrix \mathbf{I} , according to eq. (10). Therefore, the expressions for the first and second invariants are defined according to eqs. (11) and (12). The Jacobian \mathbf{J} , eq. (13), relative to the third invariant and necessary to assure the incompressibility hypothesis, is also assumed.

$$\mathbf{C} = 2\mathbf{E} + \mathbf{I} = \begin{bmatrix} 2\epsilon_{xx} + 1 & \gamma_{x\theta} & 0 \\ \gamma_{x\theta} & 2\epsilon_{\theta\theta} + 1 & 0 \\ 0 & 0 & 2\epsilon_{zz} + 1 \end{bmatrix}. \quad (10)$$

$$I_1 = \text{tr}(\mathbf{C}) = 2(\epsilon_{xx} + \epsilon_{\theta\theta} + \epsilon_{zz}) + 3. \quad (11)$$

$$I_2 = \frac{1}{2} \left\{ [\text{tr}(\mathbf{C})]^2 - \text{tr}(\mathbf{C}^2) \right\} = 4(\epsilon_{xx} + \epsilon_{\theta\theta} + \epsilon_{zz} + \epsilon_{xx}\epsilon_{\theta\theta} + \epsilon_{xx}\epsilon_{zz} + \epsilon_{\theta\theta}\epsilon_{zz}) - \gamma_{x\theta}^2 + 3. \quad (12)$$

$$I_3 = J^2 = \det(\mathbf{C}) = (2\epsilon_{zz} + 1) \left((2\epsilon_{xx} + 1)(2\epsilon_{\theta\theta} + 1) - \gamma_{x\theta}^2 \right). \quad (13)$$

The deformation-displacement relationships of eq. (14), in which ϵ_{xx} , $\epsilon_{\theta\theta}$ and $\gamma_{x\theta}$ are the components of the Green-Lagrange deformation tensor \mathbf{E} , are given by the nonlinear Sanders-Koiter theory, as presented in eqs. (15) and (16).

$$\begin{aligned} \epsilon_{xx} &= \epsilon_{x,0} + zk_x, \\ \epsilon_{\theta\theta} &= \epsilon_{\theta,0} + zk_\theta, \\ \gamma_{x\theta} &= \gamma_{x\theta,0} + zk_{x\theta}, \end{aligned} \quad (14)$$

where

$$\begin{aligned} \epsilon_{x,0} &= \frac{\partial u}{\partial x} + \frac{1}{2} \left(\frac{\partial w}{\partial x} \right)^2 + \frac{1}{8} \left(\frac{\partial v}{\partial x} - \frac{\partial u}{R\partial\theta} \right)^2 \\ \epsilon_{\theta,0} &= \frac{\partial v}{R\partial\theta} + \frac{w}{R} + \frac{1}{2} \left(\frac{\partial w}{R\partial\theta} - \frac{v}{R} \right)^2 + \frac{1}{8} \left(\frac{\partial u}{R\partial\theta} - \frac{\partial v}{\partial x} \right)^2, \\ \gamma_{x\theta,0} &= \frac{\partial u}{R\partial\theta} + \frac{\partial v}{\partial x} + \frac{\partial w}{\partial x} \left(\frac{\partial w}{R\partial\theta} - \frac{v}{R} \right) + \frac{\partial w_0}{\partial x} \left(\frac{\partial w}{R\partial\theta} - \frac{v}{R} \right), \end{aligned} \quad (15)$$

$$\begin{aligned} k_x &= -\frac{\partial^2 w}{\partial x^2}, \\ k_\theta &= \frac{\partial v}{R^2\partial\theta} - \frac{\partial^2 w}{R^2\partial\theta^2}, \\ k_{x\theta} &= -2\frac{\partial^2 w}{R\partial x\partial\theta} + \frac{1}{2R} \left(3\frac{\partial v}{\partial x} - \frac{\partial u}{R\partial\theta} \right). \end{aligned} \quad (16)$$

To represent the transverse normal strain ϵ_{zz} , the condition of Jacobian be equal to one is applied to consider the hyperelastic material as incompressible. So, with the appropriate algebra, the following equation is obtained:

$$\epsilon_{zz} = \frac{1}{2((2\epsilon_{xx} + 1)(2\epsilon_{\theta\theta} + 1) - \gamma_{x\theta}^2)} - \frac{1}{2}. \quad (17)$$

In this work, eq. (17) is expanded in terms of ϵ_{xx} , $\epsilon_{\theta\theta}$ and $\gamma_{x\theta}$ up to the fourth order, obtaining the approximated expression for ϵ_{zz} as:

$$\begin{aligned} \epsilon_{zz} \approx & -(\epsilon_{xx} + \epsilon_{\theta\theta}) + 2(\epsilon_{xx}^2 + \epsilon_{\theta\theta}^2 + \epsilon_{xx}\epsilon_{\theta\theta}) + \frac{\gamma_{x\theta}^2}{2} - 4(\epsilon_{xx}^3 + \epsilon_{\theta\theta}^3 + \epsilon_{xx}^2\epsilon_{\theta\theta} + \epsilon_{xx}\epsilon_{\theta\theta}^2) \\ & - 2(\epsilon_{xx}\gamma_{x\theta}^2 + \epsilon_{\theta\theta}\gamma_{x\theta}^2) + 8(\epsilon_{xx}^4 + \epsilon_{\theta\theta}^4 + \epsilon_{xx}^3\epsilon_{\theta\theta} + \epsilon_{xx}\epsilon_{\theta\theta}^3 + \epsilon_{xx}^2\epsilon_{\theta\theta}^2 + \epsilon_{xx}\epsilon_{\theta\theta}^2\gamma_{x\theta}^2) \\ & + 6(\epsilon_{xx}^2\gamma_{x\theta} + \epsilon_{\theta\theta}^2\gamma_{x\theta}). \end{aligned} \quad (18)$$

3 Results and discussion

A simply supported hyperelastic circular cylindrical shell of radius $R = 0.1m$, length $L = 0.1538m$, thickness $h = 0.0005m$, and density $\rho = 1100kg/m^3$ is considered. The Mooney-Rivlin material parameters are $\mu_1 = 416185.5Pa$ and $\mu_2 = -498.8Pa$. Initially, by performing a dynamic analysis, the natural frequencies and the respective vibration modes are obtained from the set of linearized equilibrium equations in eq. (2). Thus, the circumferential wave number, n , is varied, maintaining the axial half-wave number $m = 1$. The upper limits $I = J = 1$ are assumed in eq. (8) to define the modal solution for the displacement fields, disregarding the companion modal amplitudes $w_{c_{js}}(t)$ and $u_{c_{js}}(t)$. In order to validate these results, the analytical model is compared with the numerical model derived using the Finite Element Method in the commercial software Abaqus® [5]. The mesh used for the geometry under analysis is designed with 768 elements of type S4R (quadrilateral with reduced integration) that it was previously tested to guarantee the convergence of the natural frequencies. It is observed in Fig. 2 that there is convergence between the analytical model (AN - Mooney-Rivlin) and the finite element model (FEM Abaqus®) for the first five natural frequencies.

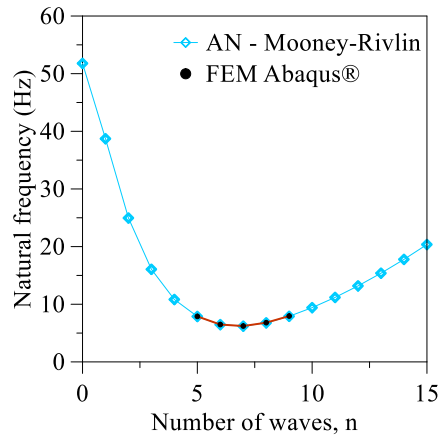


Figure 2. Frequency spectrum for the hyperelastic cylindrical shell

After the initial study of the frequencies, a forced vibration analysis is performed to evaluate the influence of the selected modes on the discretization of the displacement fields. For that, it is considered a transversal pressure magnitude $p = 0.05Pa$ and a viscous damping factor $\eta_1 = 0.03$. In this work, three models with different degrees of freedom (DOFs) are considered to define the displacement fields: Model 1 - 3 DOF ($w_{1,1}, u_{1,1}, v_{1,1}$); Model 2 - 5 DOF ($w_{1,1}, w_{1,0}, u_{1,1}, u_{1,0}, v_{1,1}$); and Model 3 - 6 DOF ($w_{1,1}, w_{c_{1,1}}, u_{1,1}, u_{c_{1,1}}, v_{1,1}, v_{c_{1,1}}$). The resonance curves are obtained, using the continuation package for dynamical analysis MatCont [6], for the models under examination, as shown in Fig. 3, in which the continuous lines refer to the stable paths and the dashed curves to the unstable ones.

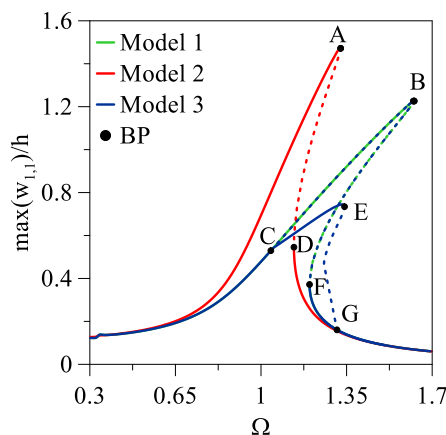


Figure 3. Resonance curves for the hyperelastic shell discretized with different modal solutions.

It is observed from Fig. 3 that Model 1, which contains only driven modes, the resonance curve initially has a stable path that extends to the peak at B, and then becomes unstable up to point F. On the other hand, Model 2, which contains the modal amplitudes of the Model 1 added by two axisymmetric modes, has similar behavior in terms of the initial stable path up to the peak A, followed by an unstable path (A-D) switching again to a stable path. It is noted that Model 1 has a higher hardening behavior than Model 2, indicating the influence of the axisymmetric mode on the increasing the softening behavior of the resonance curve of Fig. 3. The resonance curve of the axisymmetric modal amplitude $w_{1,0}$ is illustrated Fig. 4, where it is observed that its amplitude is lower than the driven mode $w_{1,1}$ but it is enough to change the nonlinear behavior of the resonance curve of Fig. 3.

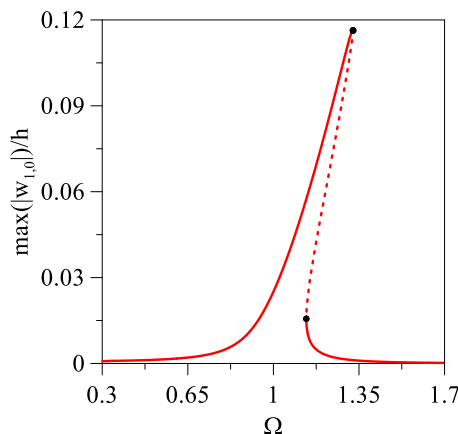


Figure 4. Resonance curves for axisymmetric mode $w_{1,0}$ of Model 2.

Now, for Model 3, which considers only the driven and companion modes, the resonance curve overlaps the curves obtained to Model 1, as presented in Fig. 3. However, the equilibrium path path C-B-F becomes unstable and there is another stable path that emerges from a bifurcation point (BP) at the point C. This new resonance peak is initially stable up to point E, and becomes unstable up to point G. It is observed that a small path F-G remains stable when it is compared with the resonance curve of Model 1. The presence of the companion mode can changes the behavior of the whole resonance curve, but only in the C-G path its modal amplitude is different from zero, as shown in Fig. 5.

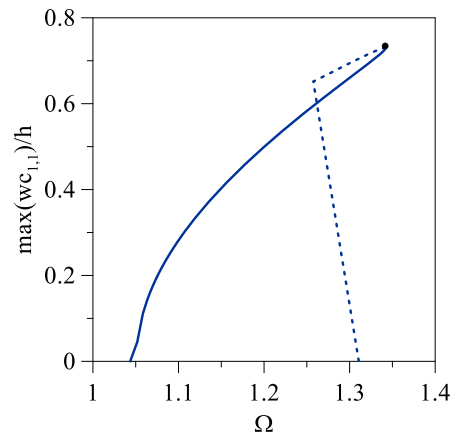


Figure 5. Resonance curve for the companion mode $wc_{1,1}$ of Model 3.

4 Conclusions

In this work, a dynamic model was developed for simply supported circular cylindrical shells composed of isotropic, homogeneous, incompressible and hyperelastic material. Both nonlinearities were considered, applying the Sanders-Koiter nonlinear shell theory (geometric nonlinearity) and the Mooney-Rivlin hyperelastic constitutive law (physical nonlinearity). The system of dynamic equations was obtained by applying the Rayleigh-Ritz method and the Euler-Lagrange equations. The initial analysis of the frequency spectrum was compatible with that determined by the FEM, validating the system of equations investigated. In the forced vibration analysis, three models were considered in order to assess the influence of different modes of the displacement fields. Model 1, with only driven modes, showed a higher hardening behavior when compared to Model 2, which contains both driven and axisymmetric modes. Model 3, on the other hand, due to the presence of the companion mode, presents a resonance curve overlapped with the resonance curve of Model 1 and a new resonance peak. It was observed that the stability of the resonance curve of Model 3 is strongly affected by the consideration of the companion mode on the displacement fields. In addition, the new resonance path was found with non-zero modal amplitudes for the companion mode. The modal coupling that occurred in the case of both Model 2 and Model 3 indicates the importance to add axisymmetric and companion modes to capture the real nonlinear behavior of the hyperelastic cylindrical shell.

Acknowledgements. The authors are grateful for the financial support provided by CAPES for the development of this work.

Authorship statement. The authors hereby confirm that they are the sole liable persons responsible for the authorship of this work, and that all material that has been herein included as part of the present paper is either the property (and authorship) of the authors, or has the permission of the owners to be included here.

References

- [1] H. B. Khaniki and M. H. Ghayesh. Highly nonlinear hyperelastic shells: Statics and dynamics. *International Journal of Engineering Science*, vol. 183, pp. 103794, 2023.
- [2] M. S. Arani, M. Bakhtiari, and A. A. Lakis. Analyzing softening and hardening behavior in vibration of a thin incompressible hyperelastic cylindrical shell. *Thin-Walled Structures*, vol. 189, pp. 110943, 2023.
- [3] F. Zheng, W. Zhang, X. G. Yuan, and Y. Zhang. Radial nonlinear vibrations of thin-walled hyperelastic under radial harmonic excitation. *Nonlinear Dynamics*, vol. 111, pp. 19791–19815, 2023.
- [4] M. Amabili. *Nonlinear Mechanics of Shells and Plates in Composite, Soft and Biological Materials*. Cambridge University Press, 2018.
- [5] Systemes Simulia Corp., Johnston, RI, USA. Abaqus Finite Element Analysis, version 2022.
- [6] W. Govaerts, Y. A. Kuznetsov, and H. G. Meijer. MatCont Numerical Bifurcation Analysis Toolbox in Matlab, version 2021 (matcont7p3).